A unified source model for the 2011 Tohoku earthquake

Kazuki Koketsu [a,*], Yusuke Yokota [a], Naoki Nishimura [b], Yuji Yagi [b], Shin'ichi Miyazaki [c], Kenji Satake [a], Yushiro Fujii [d], Hiroe Miyake [a], Shin'ichi Sakai [a], Yoshiko Yamanaka [e], Tomomi Okada [f]

[a] Earthquake Research Institute, University of Tokyo, 1-1-1 Yayoi, Bunkyo-ku, Tokyo 113-0032, Japan
[b] Department of Earth Evolution Sciences, University of Tsukuba, 1-1-1 Tennodai, Tsukuba 305-0006, Japan
[c] Department of Geophysics, Kyoto University, Kitashirakawa Oiwake-cho, Sakyo-ku, Kyoto 606-8502, Japan
[d] International Institute of Seismology and Earthquake Engineering, Building Research Institute, 1 Tatehara, Tsukuba 305-0802, Japan
[e] Research Center for Seismology, Volcanology and Disaster Mitigation, Nagoya University, Furo-cho, Chikusa-ku, Nagoya 464-8601, Japan
[f] Research Center for Prediction of Earthquakes and Volcanic Eruptions, Tohoku University, 6-6 Aza-Aoba, Aramaki, Aoba-ku, Sendai 980-8578, Japan

ARTICLE INFO

ABSTRACT

The devastating 2011 Tohoku earthquake was observed by dense networks of geophysical instruments. A unified source model was constructed through joint inversion of teleseismic, strong motion, and geodetic datasets. The result indicates that the earthquake consists of three main ruptures. After small rupture in the initial 50 s, the first rupture expanded at a slow speed of 1.8 km/s to the northeast and east. The second rupture began 20 s later at the slowest speed of 1.5 km/s and became dominant with the largest slip of 36 m. The third rupture then played the leading role, propagating southward at a speed of 2.5 km/s. Only the tsunami inversion requires an extension of the source fault to a shallow part between the first rupture area and the Japan Trench, recovering tsunamigenic slips larger than 40 m. The slow rupture speed and tsunamigenic slips can explain the features of the disaster by the earthquake.

1. Introduction

The Tohoku earthquake of 11 March 2011 (UTC) devastated huge regions, causing the Great East Japan Earthquake Disaster (Cabinet of Japan, 2011) together with large aftershocks and triggered earthquakes. This disaster resulted in 15,863 fatalities, 4414 missing, 5901 injured, and 114,591 house collapses as of 25 August 2011 (Fire Disaster Management Agency of Japan, 2011). Since more than 90% of the fatalities were from drowning (Kyodo News, 2011), and the number of injured people is relatively small, the disaster is featured by severe tsunami damage but moderate ground motion damage. Thus, it is very important to investigate the earthquake source process for exploring reasons for these features.

Its moment magnitude (M_w) of 9.0 (Japan Meteorological Agency (JMA), 2011a) to 9.1 (Global CMT Project, 2011) is the largest ever recorded in Japan and the fourth in "Largest Earthquakes in the World Since 1900" compiled by the United States Geological Survey (USGS, 2011). The earthquake is a megathrust event in a subduction zone like most others in this list, but the first that was observed by dense networks of geophysical instruments. Since abundant data obtained from these networks include teleseismic, strong motion,

geodetic, and tsunami datasets, we can construct a unified source model reflecting all aspects of the Tohoku earthquake.

2. Data

The teleseismic dataset is global and obtained from the Global Seismographic Network (GSN) through the Data Management Center of the Incorporated Research Institutions for Seismology (IRIS, 2011). The strong motion seismometers of K-NET and KiK-net (National Research Institute for Earth Science and Disaster Prevention (NIED), 2008) observed ground accelerations from the earthquake at stations shown in Fig. 1A. Gauges that observed the tsunami are also shown in Fig. 1A with the associated waveforms, though many of these stations stopped recording early because of power failure or tsunami damage. The tsunami dataset consists of these waveforms and observations at remote stations (Fujii et al., 2011). The GEONET (Geospatial Information Authority of Japan (GSI), 2010), which is a nation-wide network of 1200 GPS-based control stations, observed crustal deformations due to the earthquake as shown by static displacements in Fig. 2.

The strong motion records at 31 stations selected along the Pacific coast (red circles in Fig. 1A) were doubly integrated into ground displacements using highpass filter with a corner period of 100 s. They were aligned along the coast to form the record section in Fig. 1B. Three pulses, two of which are distinct but the other is not, can be seen in this record section, and their arrival times indicated by blue, red, and brown dots suggest that they were generated in the zones

drawn with the same colors in Fig. 1A. The first two zones are located around the epicenter of the mainshock determined by JMA (2011b), while the third zone is 150 to 180 km south of the epicenter. The static displacements in Fig. 2 point toward these zones, though they cannot distinguish the first two zones because of their limited resolving power.

Fig. 2 also shows smaller earthquakes in the 24 h after the mainshock of the Tohoku earthquake. We considered those in the black rectangular grid to be aftershocks and this rectangle of 480×150 km^2 was adopted with a strike of 200 $^\circ$ and a dip of 12 $^\circ$ to model the source fault of the mainshock. The two large events with JMA magnitudes of 7.7 and 7.4 (JMA, 2011b) were included, but some events adjacent to the western side of the rectangle were excluded, because their depths (5 to 30 km) are much shallower than the depth of the upper boundary of the subducting Pacific plate beneath them (50 to 70 km in the Japan Integrated Velocity Structure Model (JIVSM) (Koketsu et al., 2008)). On the eastern side, there is a gap between the model rectangle and the axis of the Japan Trench, as shown by a white narrow rectangle. However, we did not extend the source fault model to this area for the inversions of teleseismic, strong motion, and geodetic datasets, because there was almost no seismicity there in the 24 h after the mainshock. Another reason is that only the 1896 Sanriku earthquake is known to be a large plate-boundary event in this area and it is a typical tsunami earthquake which radiates small seismic energy but large tsunami (Kanamori, 1972; Tanioka and Satake, 1996).

3. Separate inversions

We then performed a separate inversion of each single dataset. The source fault model described in the previous section was commonly used with eighty subfaults of 30×30 km^2. Nine time windows 10 s long were assigned to every subfault, and the first time window was triggered at a time calculated with a distance from the rupture initiation point and a velocity of 2.5 km/s. The epicenter and origin time determined by JMA (2011b) were used as the location and time of rupture initiation. The focal depth of the mainshock is relocated at a depth of 17 km to follow the subducting Pacific plate of the JIVSM. When a layered velocity structure was required for the inversions, we extracted it from the JIVSM.

For the inversion of the teleseismic dataset using the method of Yagi and Fukahata (2008) and Green's functions of Kikuchi and Kanamori (1991), we selected GSN stations at epicentral distances of 30° to 100° (Fig. 3A), removed instrumental responses from *P*-wave records observed at these stations, and integrated them into ground displacements using a bandpass filter of 4 to 500 s. For the inversion of the strong motion dataset using the method of Yoshida et al. (1996) with the revisions of Hikima and Koketsu (2005) and Green's functions of Kohketsu (1985), we selected 20K-NET/KiK-net stations (Fig. 3B) from those plotted in Fig. 1, applied a bandpass filter of 10 to 100 s to three-component records, and integrated them into ground velocities. For the inversion of the geodetic dataset using the method of Miyazaki and Larson (2008) and Green's functions of
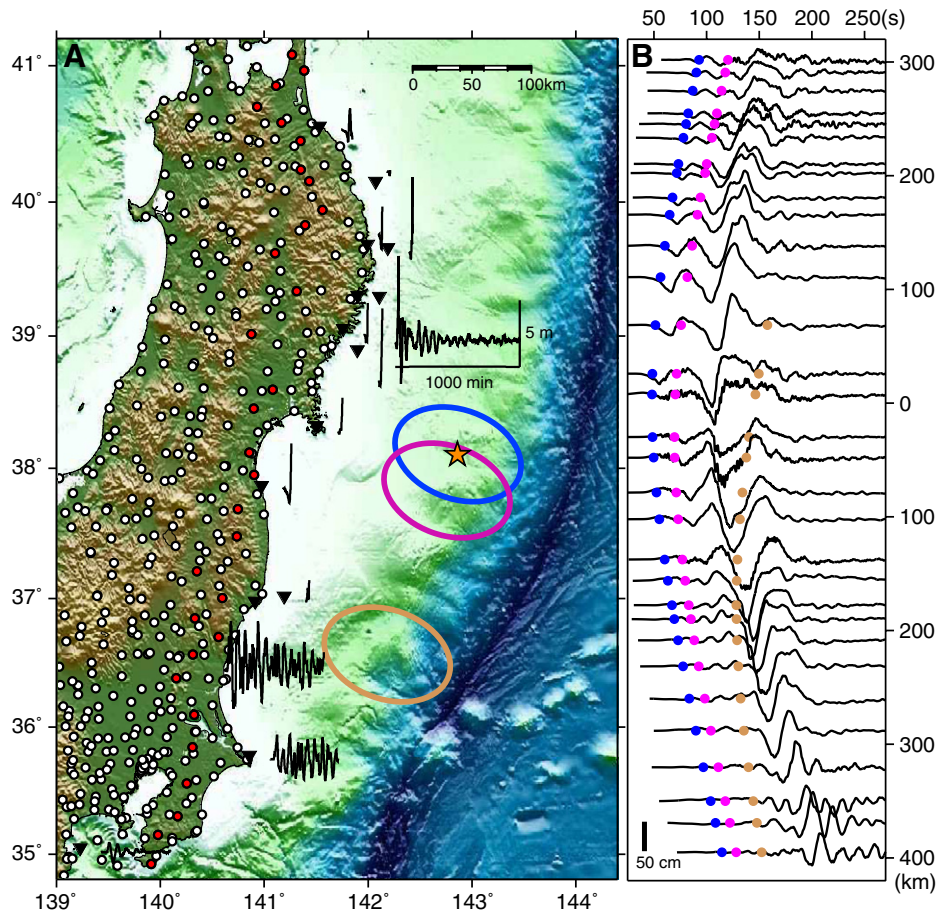
Fig. 1. (A) Strong motion stations operated by NIED (small white and red circles) and local tsunami gauges (black inverted triangles) associated with observed waveforms (black traces). The orange star denotes the epicenter determined by JMA. (B) Section of ground displacements obtained by double integration of accelerations observed at the red stations. Three pulses can be seen and their arrival times (blue, red, and brown dots) suggest three zones of large slip (blue, red, and brown ellipses in the panel A).
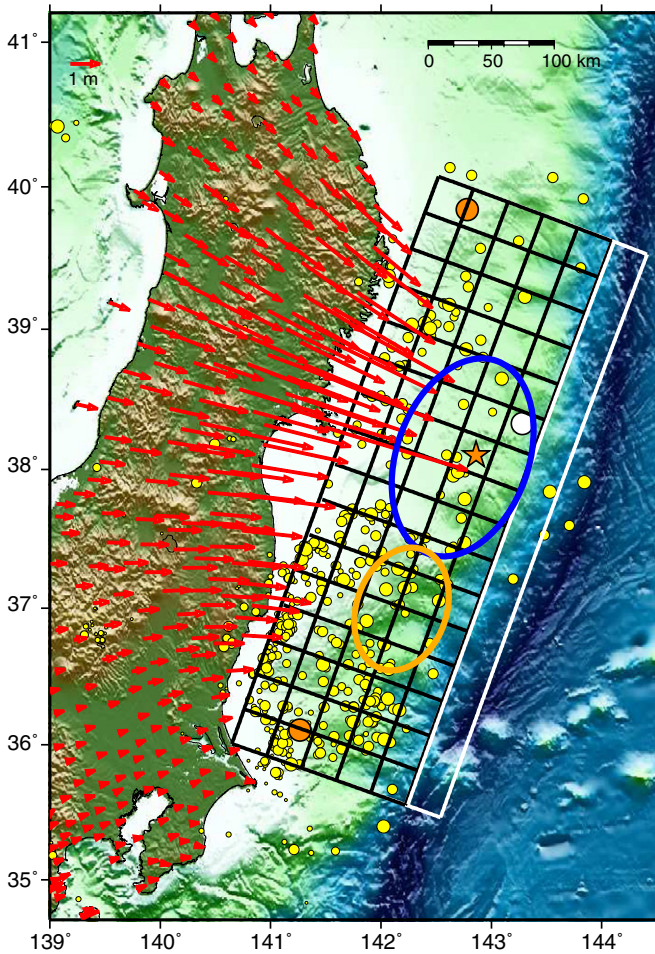
Fig. 2. Horizontal static displacements observed by GEONET (red arrows) suggest two zones of large slip (blue and brown ellipses). The source fault (rectangular grid) is assumed based on the distribution of smaller earthquakes during the initial 24 h (yellow circles). The orange star, orange and white circles denote the epicenters of the mainshock, aftershocks with magnitudes greater than 7.0, and a foreshock, respectively. The white narrow rectangle is an extension of the source fault for the tsunami inversion.

distribution by the geodetic inversion. There is no large slip in the southernmost parts of the slip distributions by the strong motion and geodetic inversions, while some considerable slips are recovered in the slip distribution by the teleseismic inversion. These differences are mostly due to the low resolution of the geodetic and teleseismic inversions (Fig. S1). We also noted that the JIVSM was used for Green's functions of the teleseismic and strong motion inversions; however just a halfspace was used for those of the geodetic and tsunami inversions. This may have affected the comparison of the results of the separate inversions.

Okada (1985), we selected 16 GEONET stations (Fig. 3B) from those plotted in Fig. 2, and calculated two-component static displacements by comparing averages before and immediately after the mainshock. For the inversion of the tsunami dataset using the method of Yoshida et al. (1996) with the revisions of Hikima and Koketsu (2005) and Green's functions of Fujii and Satake (2007), we removed tidal components from tsunami records (Figs. 1A and 3A) using polynomial functions approximation, and resampled them at 1 min intervals.

The separate inversions of the teleseismic, strong motion, and geodetic datasets successfully provided stable solutions as shown by the resultant slip distributions in Fig. 4A, B, and C. Using the rigidity structure derived from the JIVSM, their seismic moments are calculated to be 5.3×10^{22} Nm (M_w 9.1), 3.4×10^{22} Nm (M_w 9.0), and 3.7×10^{22} Nm (M_w 9.0), respectively. However, the tsunami inversion with our source fault model did not provide a stable solution. It requires a modification of the source fault model.

Although the stable solutions of the three separate inversions in Fig. 4A, B, and C are all based on the common source fault model and all find the largest slip in the central part of the rupture, there are considerable differences in other details. For example, the strong motion and teleseismic inversions recovered two zones of large slip, while they are combined into a single large zone in the slip

Fig. 3. (A) GSN stations (black triangles) and remote tsunami stations (black inverted triangles) observing the data used in the teleseismic and tsunami inversions, respectively. (B) K-NET/KiK-net stations (blue circles), GEONET stations (red circles), and local tsunami stations (black inverted triangles) observing the data used in the strong motion, geodetic, and tsunami inversions, respectively. The source fault model (black grid) is also shown with the mainshock epicenter (orange star).
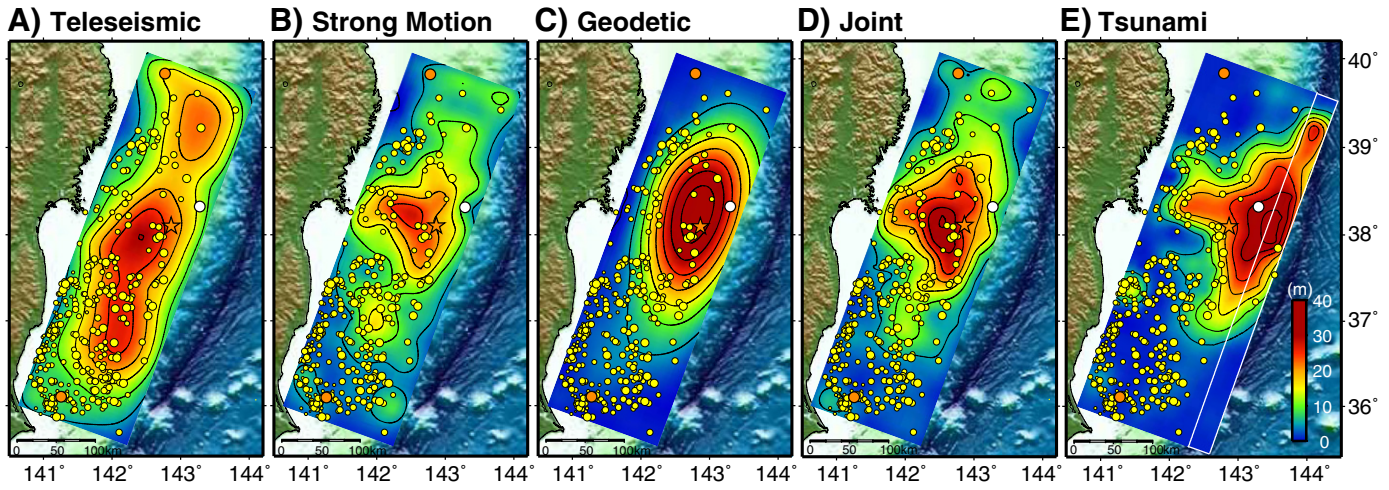
Fig. 4. Slip distributions obtained by the inversions of the (A) teleseismic, (B) strong motion, and (C) geodetic datasets. (D) The slip distribution from the joint inversion of the teleseismic, strong motion, and geodetic dataset is compared with (E) that from the inversion of tsunami dataset. The white narrow rectangle in (E) is an extension of the source fault for the tsunami inversion. The yellow circles represent aftershocks in the initial 24 h. The orange star, orange and white circles denote the epicenter of the mainshock, aftershocks with magnitudes greater than 7.0, and a foreshock, respectively.

4. Unified source model

Because ground motions and deformations observed by seismometers and GPS receivers are elastic consequences of the earthquake, we assumed that the teleseismic, strong motion and geodetic datasets could provide similar slip distributions, despite of the minor differences mentioned above. Accordingly, in order to construct a unified source model, we carried out a triple joint inversion of the teleseismic, strong motion, and geodetic datasets using the method of Yoshida et al. (1996) with the revisions of Hikima and Koketsu (2005) and Green's functions of Kikuchi and Kanamori (1991), Kohketsu (1985), and Zhu and Rivera (2002), respectively. The slip distribution by

the strong motion inversion is in the best agreement with the zones suggested by the record section in Fig. 1A and distribution of static displacements in Fig. 2; therefore a 17% larger weight was assigned to the strong motion dataset than the others.

We obtained the unified source model (Fig. 4D) through this joint inversion. Using the rigidity structure derived from the JIVSM, the seismic moment of the model is calculated to be 3.8×10^{22} Nm, which yields $M_w = 9.0$. Figs. 5 to 7 compare the observations and synthetics for the teleseismic, strong motion, and geodetic datasets, respectively, showing good performance of the unified source model. In the slip distribution of the model, large slips are well recovered again at the areas which correspond to the zones of large slip
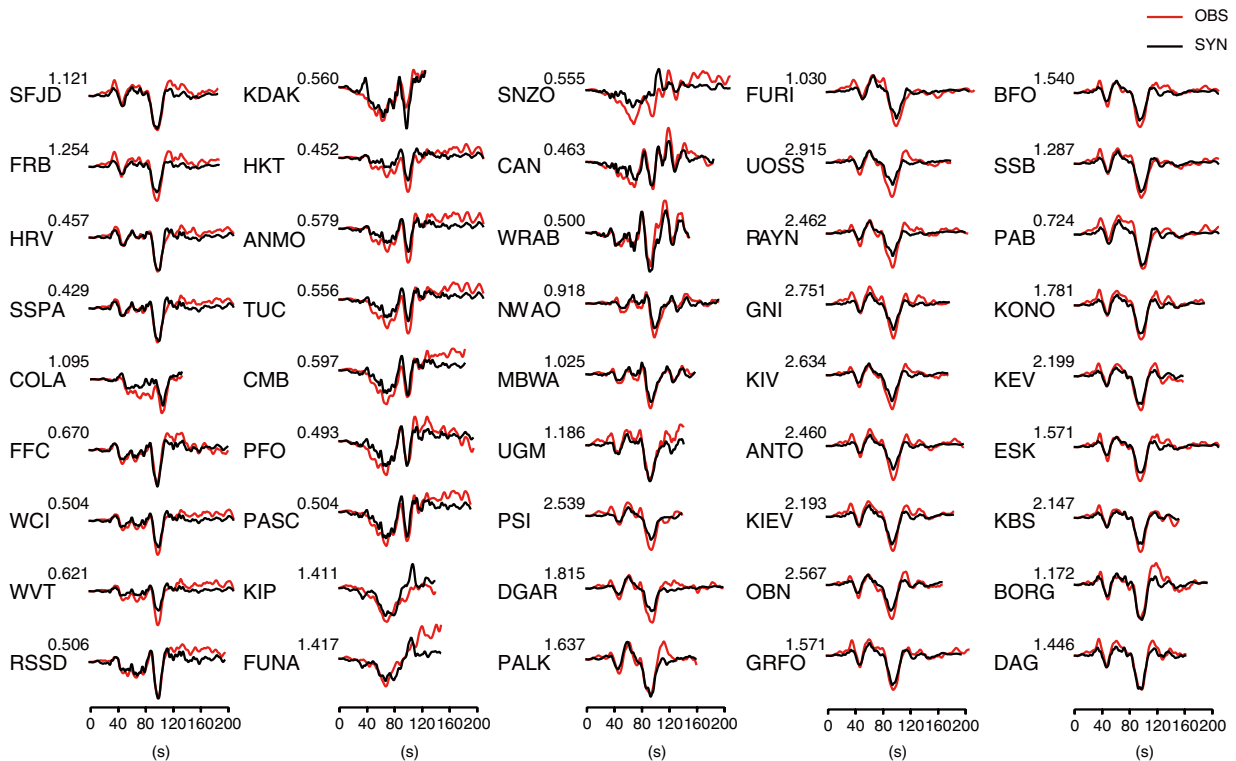
Fig. 5. Comparison of the observed (red) and synthetic (black) teleseismic waveforms for the result of the joint inversion. Amplitudes are written in mm after station codes.

suggested in Figs. 1 and 2. The aftershocks can be seen to surround these large slips. From the total seismic moment and whole source fault area, the stress drop is calculated to be as high as 4.8 MPa using the circular crack approximation of Eshelby (1957). The zones of large slip include the Miyagi-oki region, for which the Earthquake Research Committee of the Japanese government reported the probability of having another M7 earthquake during the 30 year period to be greater than 90%. The Tohoku earthquake caused 15 to 20 m slip in this region, and thus that prediction has been partially fulfilled. However, the total size of the earthquake is much larger than an M7 event, as Kanamori et al. (2006) anticipated from the difference between the seismic slip rate and plate motion rate.

Since the seafloor displacements observed by a GPS/acoustic combination technique were recently published (Sato et al., 2011), we performed a blind prediction of seafloor displacements using the Green's functions mentioned in Section 3 and the coseismic slip distribution in Fig. 4D. These observations and prediction results are in surprisingly good agreement with each other as shown in Fig. 8, even though the observations were not used in the joint inversion. This agreement confirms the validity of the joint inversion result.

From the unified source model, we made snapshots of slip distribution every 10 s after the rupture initiation for illustrating the progress of the source rupture. The snapshots in Fig. 9 indicate that the earthquake consists of three main ruptures, which again correspond to the zones of large slip suggested in Figs. 1 and 2. After small rupture for the initial 50 s, the first rupture expanded at a slow speed of 1.8 km/s to the northeast and east (red arrows at 50–60 s). 20 s later the second rupture began to propagate westward at the slowest speed of 1.5 km/s and became dominant with the largest final slip of 36 m (blue arrow at 70–80 s). Therefore, the first and second ruptures result in bilateral rupture propagation in the dip direction. The third rupture then played the leading role, propagating southward at a speed of 2.5 km/s (purple arrow at 90–100 s). In addition, the first rupture turned to the north at about 60 s and propagated northward

at this speed, so that the later first and third ruptures resulted in bilateral rupture propagation in the strike direction.

5. Tsunami inversion

In order to obtain a stable solution of the tsunami inversion, we extended the source fault model to the shallowest part of the plate boundary neighboring the Japan Trench, as shown by the white narrow rectangle in Fig. 2. This extension is 30 km wide and dipping with an angle of 7.5 °. The solution for the extended source fault model is shown in Fig. 4E. The seismic moment of this solution is 3.4×10^{22} Nm (M_w 9.0). The synthetic tsunami waveforms for this solution are in good agreement with the observed ones as shown in Fig. 10.

Comparing Fig. 4E and D, we found that the slip distribution in the 480×150 km^2 part of the tsunami inversion result (Fig. 4E) resembles the slip distribution of the unified source model (Fig. 4D). This implies that the slips larger than 40 m on the fault extension to the trench are tsunamigenic but not effective to cause ground motions and static displacements. Therefore, we may construct a more complete unified source model by adding these tsunamigenic slips to the current unified source model.

However, the slip distribution in Fig. 4E does not hold the common feature of Fig. 4A to C, which is that the largest slip is found in the central part of the rupture. This is the reason why we did not include the tsunami dataset in the joint inversion. The largest slip of the tsunami inversion result (Fig. 4E) is located in the easternmost part of the source fault, which is the fault extension to the Japan Trench.

The comparison of the snapshots at 50–60 s and 60–70 s (Fig. 9) with the result of the tsunami inversion (Fig. 4E) suggests that the early first rupture stimulated the fault extension to the trench and caused the large tsunamigenic slips. Note that the M_w 7.4 foreshock on 9 March 2011 (white circle in Figs. 2 and 4) is located in a zone connecting the early first rupture and the fault extension.
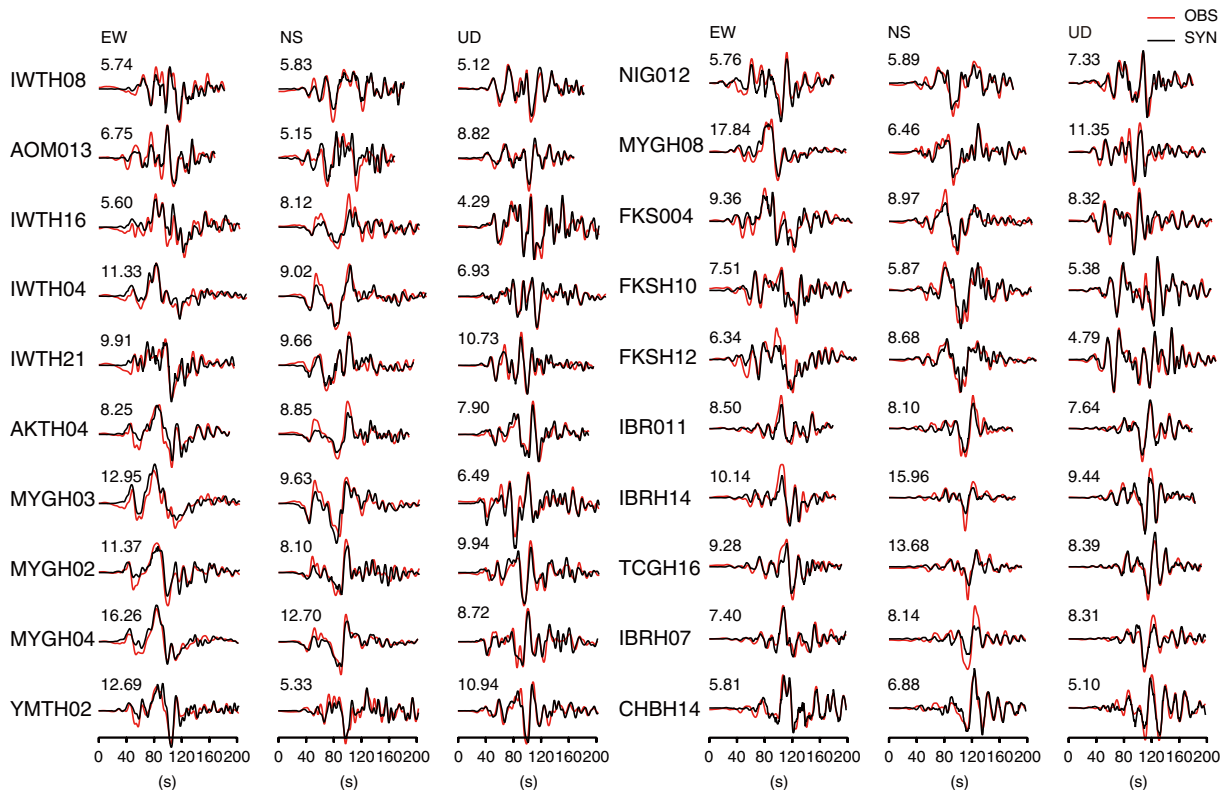
Fig. 6. Comparison of the observed (red) and synthetic (black) strong motion waveforms for the result of the joint inversion. Amplitudes are written in cm/s after station codes.
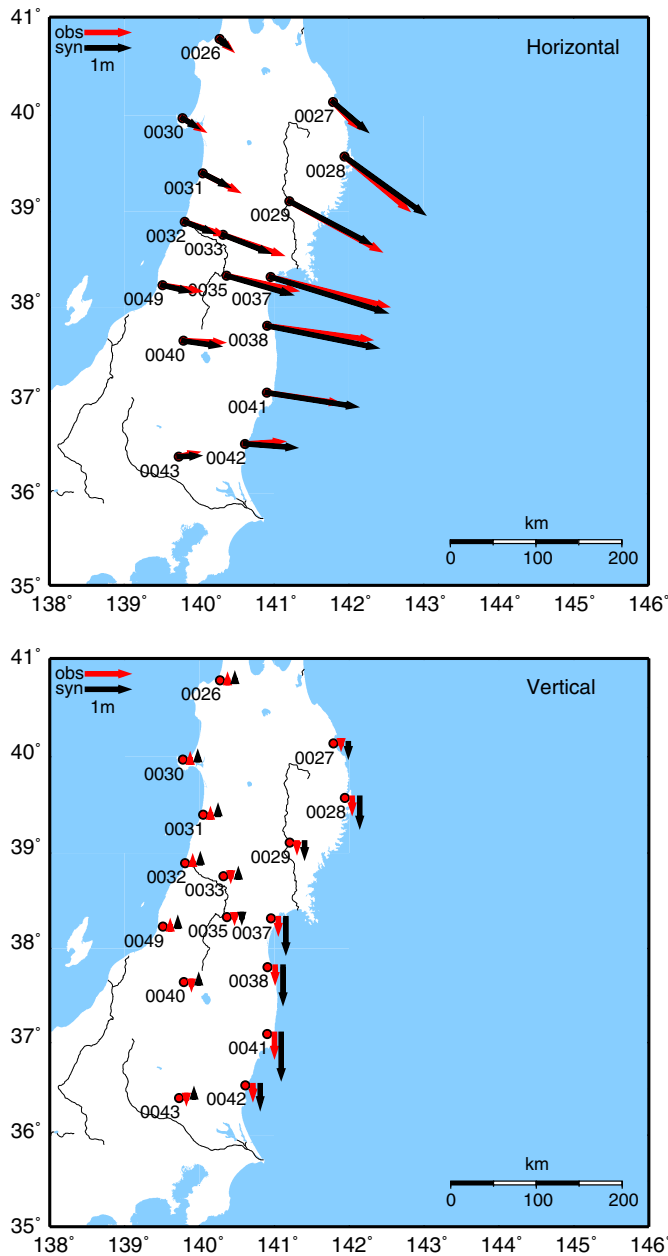
Fig. 7. Comparison of the observed (red) and synthetic (black) static displacements for the result of the joint inversion in the horizontal (Upper) and vertical (Lower) components.

6. Conclusions and discussion

Previous megathrust events such as the 1952 M_w 9.0 Kamchatka, 1960 M_w 9.5 Chile, 1964 M_w 9.2 Alaska, and 2004 M_w 9.1 Sumatra–Andaman earthquakes ruptured largely unilaterally over 800 to 1300 km long areas (e.g., Ishii et al., 2005). However, the 2011 Tohoku earthquake ruptured bilaterally over the compact area only 480 km long, which resulted in the high stress drop of 4.8 MPa. A recent Chilean megathrust event called the 2010 M_w 8.8 Maule earthquake also ruptured bilaterally, but its extent is as long as 650 km (e.g., Lorito et al., 2011).

The propagation speed of the first and second main ruptures is as slow as 1.5–1.8 km/s, which is comparable to that at the initial stage of the Sumatra–Andaman earthquake (Ammon et al., 2005). The slow rupture growth of the earthquake source required larger fracture

energy, therefore the resultant radiated energy became smaller based on the energy budget (Kanamori and Heaton, 2000). Thus, one feature of this earthquake disaster, that is moderate ground motion damage, can be explained by the slow rupture speed. Since the 2010 Maule earthquake also has a slightly slow rupture speed of 2.25 km/s (Lorito et al., 2011), slow rupture growth may be a common phenomenon for megathrust events in subduction zones.

The other feature, that is severe tsunami damage, can be explained by the tsunamigenic slips mentioned in Section 5. Since Tanioka and Seno (2001) already found this kind of deformation effective only on tsunami generation in the 1896 Sanriku tsunami earthquake, the 2011 Tohoku earthquake may be a combination of a megathrust event in the 480×150 km^2 part and a large tsunami earthquake in the area neighboring the Japan Trench. Minoura et al. (2001) found the 869 Jogan earthquake to have occurred with a magnitude similar to that of the 2011 Tohoku earthquake, and Satake et al. (2008) located its source fault in the 480×150 km^2 part.

A 'first generation' of source models for the 2011 Tohoku earthquake have now been published. Among them, several models by inversions of teleseismic data only (Hayes, 2011; Ide et al., 2011; Lay et al., 2011; Shao et al., 2011) show slip distributions different from those of our joint and separate inversions. They each have a peak slip zone in the east of the epicenter, closely to the Japan Trench. The resolution of a teleseismic-data-only inversion is low everywhere in the source region as shown in Fig. S1; hence both a peak slip zone neighboring the trench and one around the epicenter such as in Fig. 4a can provide fairly good waveform fits. However, Sato et al. (2011) observed large horizontal displacements of 23–24 m (Fig. 8) and small upward displacements of 1.5–3 m, around the epicenter. These observations support our slip distribution with a peak slip zone around the epicenter.

We did not carry out a fourfold joint inversion of the three datasets and the tsunami dataset by expanding the source fault model to that for the tsunami inversion, because the three separate inversions and threefold joint inversion using the expanded source fault model provided only similar results to those in Fig. 4A to D. We would like to keep the fourfold joint inversion for future works.
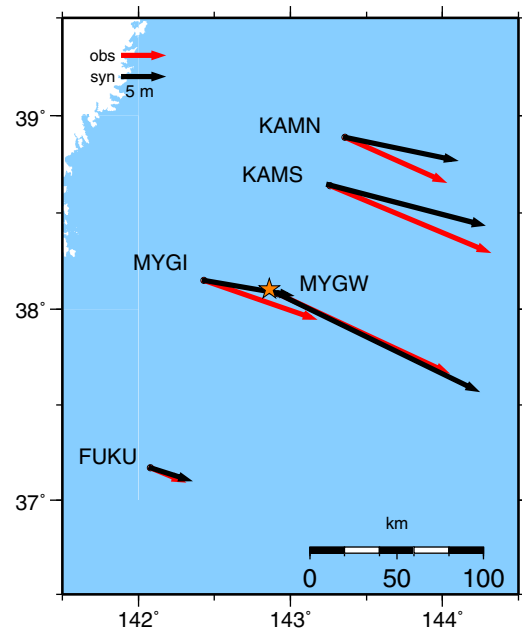
Fig. 8. Comparison of the observed (red) and predicted (black) seafloor displacements. The observed ones were obtained by seafloor geodetic observations using a GPS/acoustic combination technique (Sato et al., 2011), while the predicted ones were computed using the coseismic slip distribution in Fig. 4D. The orange star denotes the epicenter of the mainshock.
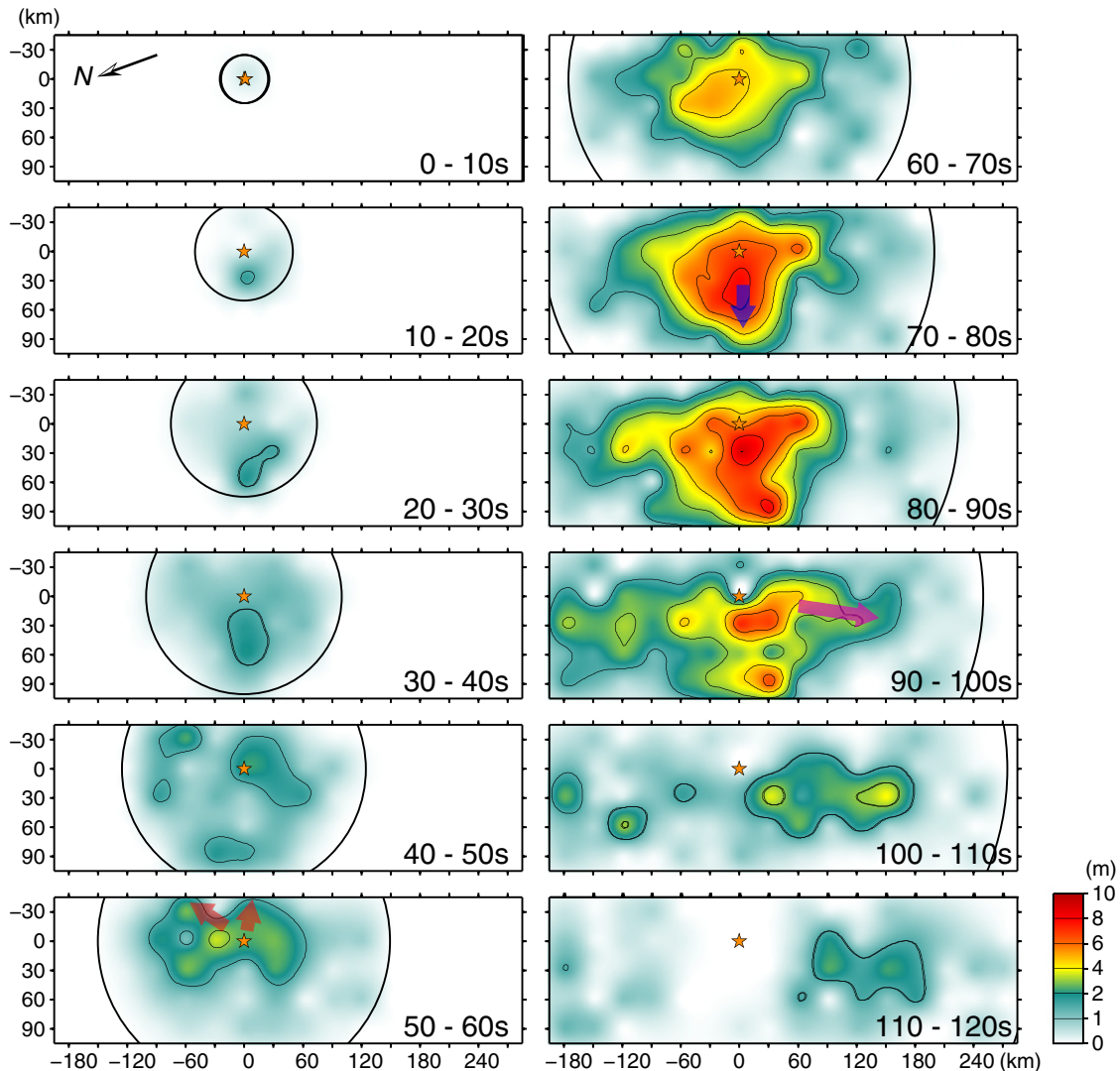
Fig. 9. Progress of the source rupture represented by snapshots of slip distribution of the joint inversion at every 10 s after rupture initiation at the JMA hypocenter (orange star). Black circles indicate rupture propagation at a speed of 2.5 km/s. Red, blue, and purple arrows schematically illustrate the propagation of three main ruptures.

Supplementary materials related to this article can be found online at doi:10.1016/j.epsl.2011.09.009.

Fig. S1. Results of the checkerboard resolution tests for the joint and separate inversions of the teleseismic, strong motion, geodetic, and tsunami datasets. The target slip distributions are shown in the leftmost column.

References

Ammon, C.J., Ji, C., Thio, H.-K., Robinson, D., Ni, S., Hjorleifsdottir, V., Kanamori, H., Lay, T., Das, S., Helmberger, D., Ichinose, G., Polet, J., Wald, D., 2005. Rupture process of the 2004 Sumatra–Andaman earthquake. Science 308, 1133–1139.

Cabinet of Japan, 2011. Press Conference by Prime Minister Naoto Kan. http://www.kantei.go.jp/foreign/kan/statement/201104/01kaiken_e.html 2011.

Eshelby, J.D., 1957. The determination of the elastic field of an ellipsoidal inclusion and related problems. Proc. R. Soc. A241, 376–396.

Fujii, Y., Satake, K., 2007. Tsunami source of the 2004 Sumatra–Andaman earthquake inferred from tide gauge and satellite data. Bull. Seismol. Soc. Am. 97, S192–S207.

Fujii, Y., Satake, K., Sakai, S., Shinohara, M., Kanazawa, T., 2011. Tsunami source of the 2011 off the Pacific coast of Tohoku, Japan earthquake, Earth Planets Space 63. doi:10.5047/eps.2011.06.010.

Fire Disaster Management Agency of Japan, 2011. The 137th report (25 August 2011). http://www.fdma.go.jp/bn/2011/detail/691.html 2011.

Global CMT Project, 2011. Global CMT Catalog Search. http://www.globalcmt.org/CMTsearch.html 2011.

GSI, 2010. Geodetic survey. http://www.gsi.go.jp/ENGLISH/page_e30030.html 2010.

Hayes, G. P., 2011. Rapid source characterization of the 03-11-2011 Mw 9.0 Off the Pacific Coast of Tohoku earthquake, Earth Planets Space 63, doi:10.5047/eps.2011.05.012.

Hikima, K., Koketsu, K., 2005. Rupture processes of the 2004 Chuetsu (mid-Niigata prefecture) earthquake, Japan: A series of events in a complex fault system. Geophys. Res. Lett. 32, L18303. doi:10.1029/2005GL023588.

Ide, S., Baltay, A., Beroza, G.C., 2011. Shallow dynamic overshoot and energetic deep rupture in the 2011 M_w 9.0 Tohoku-Oki earthquake. Science 332, 1426–1429.

IRIS, 2011. Data Management Center. http://www.iris.edu/dms/dmc/ 2011.

Ishii, M., Shearer, P.M., Houston, H., Vidale, J.E., 2005. Extent, duration and speed of the 2004 Sumatra–Andaman earthquake imaged by the Hi-Net array. Nature 485, 933–936.

JMA, 2011a. The 2011 off the Pacific coast of Tohoku Earthquake ~28th report~. http://www.jma.go.jp/jma/press/1103/25b/201103251730.html 2011.

JMA, 2011b. Seismological and Volcanological Bulletin of Japan for March 2011. http://www.hinet.bosai.go.jp/REGS/JMA/list/ 2011.
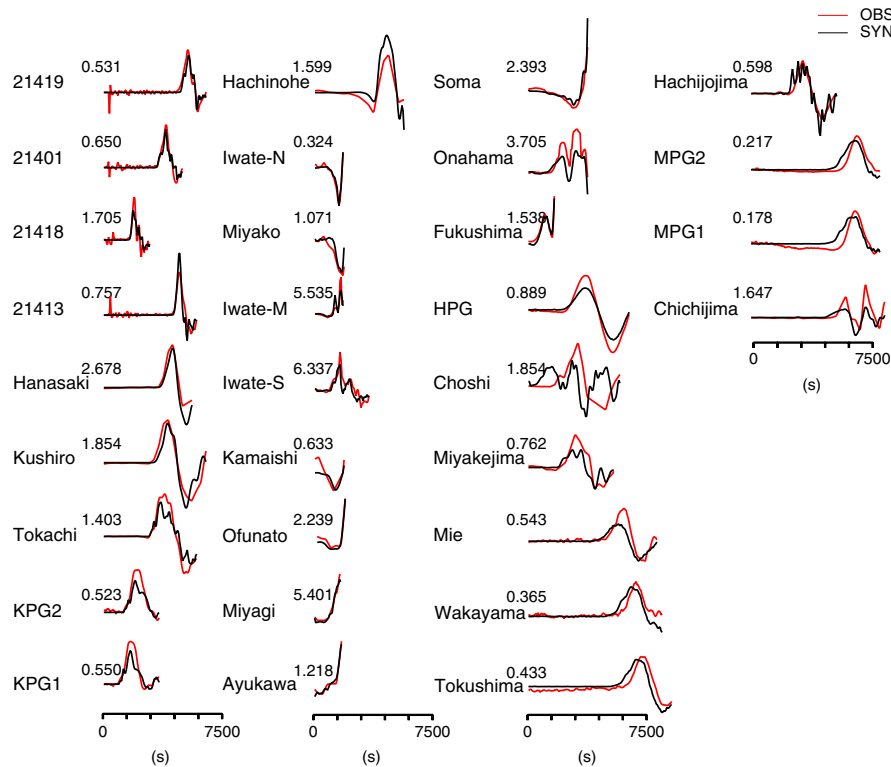
Fig. 10. Comparison of the observed (red) and synthetic (black) tsunami waveforms for the result of the separate inversion of the tsunami dataset. Amplitudes are written in m after station codes.

Kanamori, H., 1972. Mechanism of tsunami earthquakes. Phys. Earth Planet. Inter. 6, 346–359.

Kanamori, H., Heaton, T.H., 2000. Microscopic and macroscopic physics of earthquakes. GeoComplexity and the Physics of Earthquakes: Geophysical Monograph, 120, pp. 147–163.

Kanamori, H., Miyazawa, M., Mori, J., 2006. Investigation of the earthquake sequence off Miyagi prefecture with historical seismograms. Earth Planets Space 58, 1533–1541.

Kikuchi, M., Kanamori, H., 1991. Inversion of complex body waves—III. Bull. Seismol. Soc. Am. 81, 2335–2350.

Kohketsu, K., 1985. The extended reflectivity method for synthetic near-field seismograms. J. Phys. Earth 33, 121–131.

Koketsu, K., Miyake, H., Fujiwara, H., Hashimoto, T., 2008. Progress towards a Japan integrated velocity structure model and long-period ground motion hazard map. Proceedings of the 14th World Conference on Earthquake Engineering, abstract S10–038.

Kyodo News, 2011. Over 90% of March 11 victims died from drowning. http://www.japantoday.com/category/national/view/over-90-of-march-11-victims-died-from-drowning-npa 2011.

Lay, T., Ammon, C. J., Kanamori, H., Xue, L., Kim, M. J., 2011. Possible large near-trench slip during the great 2011 Tohoku (M_w 9.0) earthquake, Earth Planets Space 63. doi:10.5047/eps.2011.05.033.

Lorito, S., Romano, F., Atzori, S., Tong, X., Avallone, A., McCloskey, J., Cocco, M., Boschi, E., Piatanesi, A., 2011. Limited overlap between the seismic gap and coseismic slip of the great 2010 Chile earthquake. Nat. Geosci. 4, 173–177.

Minoura, K., Imamura, F., Sugawara, D., Kono, Y., Iwashita, T., 2001. The 869 Jogan tsunami deposit and recurrence interval of large-scale tsunami on the Pacific coast of northeast Japan. J. Nat. Disaster Sci. 23, 83–88.

Miyazaki, S., Larson, K., 2008. Coseismic and early postseismic slip for the 2003 Tokachi-oki earthquake sequence inferred from GPS data. Geophys. Res. Lett. 35, L04302. doi:10.1029/2007GL032309.

NIED, 2008.(K-NET, KiK-net). http://www.kyoshin.bosai.go.jp/index_en.html2011.

Okada, Y., 1985. Surface deformation due to shear and tensile faults in a half-space. Bull. Seismol. Soc. Am. 75, 1135–1154.

Satake, K., Namegaya, Y., Yamaki, S., 2008. Numerical simulation of the AD 869 Jogan tsunami in Ishinomaki and Sendai plains. Annu. Rep. Active Fault Paleoearthquake Res. 8, 71–89 (in Japanese with English abstract).

Sato, M., Ishikawa, T., Ujihara, N., Yoshida, S., Fujita, M., Mochizuki, M., Asada, A., 2011. Displacement above the hypocenter of the 2011 Tohoku-Oki earthquake. Science 332, 1395.

Shao, G., Li, X., Ji, C., Maeda, T., 2011. Focal mechanism and slip history of 2011 M_w 9.1 off the Pacific coast of Tohoku Earthquake, constrained with teleseismic body and surface waves, Earth Planets Space 63. doi:10.5047/eps.2011.06.028.

Tanioka, Y., Satake, K., 1996. Fault parameters of the 1896 Sanriku tsunami earthquake estimated from tsunami numerical modeling. Geophys. Res. Lett. 23, 1549–1552.

Tanioka, Y., Seno, T., 2001. Sediment effect on tsunami generation of the 1896 Sanriku tsunami earthquake. Geophys. Res. Lett. 28, 3389–3392.

USGS, 2011. Largest Earthquakes in the World Since 1900. http://earthquake.usgs.gov/earthquakes/world/10_largest_world.php 2011.

Yagi, Y., Fukahata, Y., 2008. Importance of covariance components in inversion analyses of densely sampled observed data: an application to waveform data inversion for seismic source processes. Geophys. J. Int. 175, 215–221.

Yoshida, S., Koketsu, K., Shibazaki, B., Sagiya, T., Kato, T., Yoshida, Y., 1996. Joint inversion of the near- and far-field waveforms and geodetic data for the rupture process of the 1995 Kobe earthquake. J. Phys. Earth 44, 437–454.

Zhu, L., Rivera, L.A., 2002. A note on the dynamic and static displacements from a point source in multilayered media. Geophys. J. Int. 148, 619–627.